ACS OMEGA

Article

Cite This: ACS Omega 2018, 3, 8271−8277

http://pubs.acs.org/journal/acsodf

Enhanced Aerosol Particle Filtration Efficiency of Nonwoven Porous Cellulose Triacetate Nanofiber Mats

Ratna Balgis,[†] Hiroyuki Murata,[†] Takashi Ogi,*[,†] Makoto Kobayashi,[‡] and Li Bao[‡]

[†]Department of Chemical Engineering, Graduate School of Engineering, Hiroshima University, 1-4-1 Kagamiyama, Higashi, Hiroshima 739-8527, Japan

[‡]Nippon Muki Co., Ltd., Nisshin Ueno Building, 5-1-5 Higashi-Ueno, Tokyo 110-0015, Japan

Supporting Information

ABSTRACT: Aerosol particle filtration in most penetrating particle size (MPPS) region is of great challenge for conventional nonwoven filter mats. The present work, therefore, redesigns conventional filter mats by introducing porous structure. A combination of thermally induced phase separation and breath figure mechanism was employed to synthesize porous cellulose triacetate fibers, in conjunction with the volatile solvent methylene chloride. The ambient humidity, the concentration of the polyvinylpyrrolidone (PVP) secondary polymer, and the ethanol cosolvent were all adjusted to modify the Taylor cone formation, jet stability, and fiber porosity. After fiber formation, the PVP was removed to obtain a superhydrophobic material. To distinguish the effect of pores, the performance of porous and nonporous nanofibers having similar sizes was conducted. Tests were performed using various dust particle sizes, and the results show that the collection efficiency of the porous fibers, resulting from particle diffusion, inertial impaction, and interception, was improved. Interestingly, the efficiency of the porous fibers in the MPPS region was exceptionally enhanced (up to 95%), demonstrating that the presence of dynamic pores greatly contributes to particle capture.

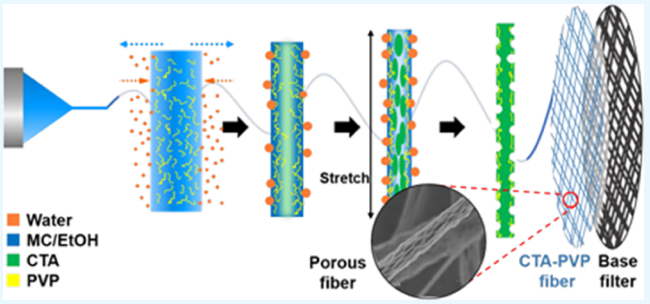

1. INTRODUCTION

The use of electrospun nonwoven fiber mats with high specific surface areas could lead to greatly improved performance in many different applications, including biotechnology membranes, air filtration, sensors, tissue engineering and repairs, drug delivery, and solar and fuel cells.[1−7] Unlike conventional rigid porous structures, these porous structures made from nonwoven fibers mats are dynamic systems in which both pore size and shape can change.[8,9] Multilevel-structured fibers mats are also attractive because they offer additional heterogeneous interfaces that can play important roles in a variety of practical applications.[10,11]

Many researchers have successfully fabricated nonwoven porous fiber mats from various polymers by a number of different methods, including electrospinning.[12,13] The filtration performance for a particle size >0.25 μm has also been reported. However, a lack of information regarding the structure−performance relationship in such porous fibers remains an obstacle, particularly in the most penetrating particle size (MPPS) region of the filtration evaluation. It is also not clear to what extent the aerosol filtration performance is enhanced by the presence of pores or the formation of nanofiber. For these reasons, the present study examined the correlations between porous structure and aerosol filtration performance through various filtration mechanisms.

Cellulose triacetate (CTA) was chosen for this work because it is superhydrophobic and thus suitable for aerosol particle filtration and can also be dissolved in highly volatile solvents such as methylene chloride (MC).[14] A combination of thermally induced phase-separation and the breath-figure mechanism was employed to fabricate test specimens. In addition, ethanol (EtOH) was used as a cosolvent to control the MC evaporation rate so that polymer stretching could be achieved.[15,16] Because porous and nonporous (NP) fibers were compared, this investigation is expected to improve our understanding of the structure−property relationship in terms of aerosol filtration performance. Various sizes of dust particles were employed to carefully evaluate the filtering ability, based on particle diffusion, inertial impaction, and interception, and the MPPS region.

2. RESULTS AND DISCUSSION

2.1. Morphologies of CTA Nanofibers and Effects of CTA Concentration and Humidity. The electrospinning characteristics of a polymer are affected by its physical properties, including electrical conductivity, surface tension, and viscosity.[17,18] Solvent selection is also important in

Received: April 10, 2018
Accepted: June 8, 2018
Published: July 25, 2018

DOI: 10.1021/acsomega.8b00695
ACS Omega 2018, 3, 8271−8277

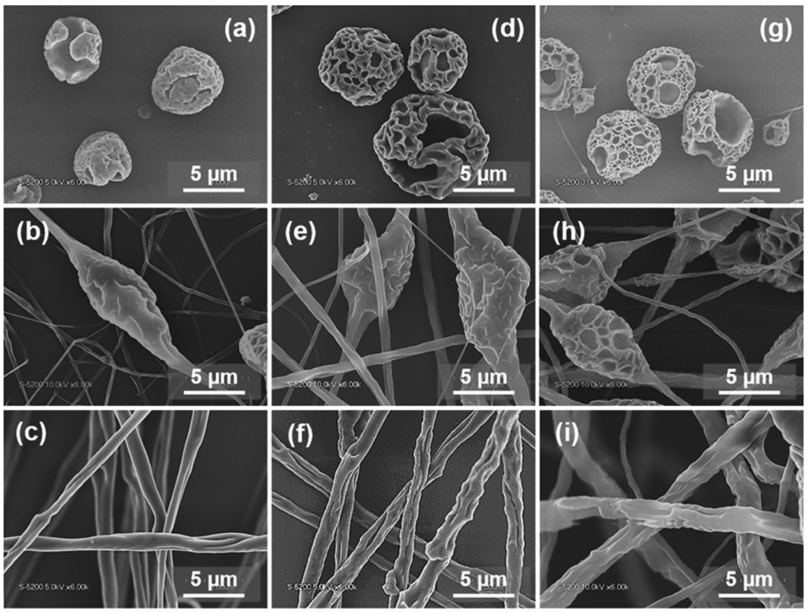

Figure 1. Scanning electron microscopy (SEM) images of CTA spun at a relative humidity of 35% from solutions containing (a) 3, (b) 5, and (c) 7 wt % CTA, at a relative humidity of 50% from solutions containing (d) 3, (e) 5, and (f) 7 wt % CTA, and at a relative humidity of 70% from solutions containing (g) 3, (h) 5, and (i) 7 wt % CTA, respectively. Polymer precursors were made using MC/EtOH ratios (vol/vol) of 90/10 as the solvent.

determining the formation of a Taylor cone and in adjusting the polymer elongation.[19] A low boiling-point solvent will evaporate rapidly (almost immediately after ejection from the needle), thus restricting polymer elongation and leading to either a clogged needle or a scattered Taylor cone.[14] In contrast, a high viscosity precursor can slow the evaporation of the solvent. Therefore, finding the appropriate balance between the solvent evaporation rate and the viscosity of the polymer precursor is vital to obtain well-structured fibers.

Polymer precursors with various concentrations of CTA and solvent of MC/EtOH ratios (vol/vol) of 90/10 were evaluated. The viscosities of the polymer precursors were found to increase in proportion to the CTA concentration, with values of 21, 101, and 305 cp for 3, 5, and 7 wt % CTA, respectively. As shown in Figure 1a–c, the morphology of the electrospun precursor was transformed from dented surface particles to beaded fibers and finally to fibers with dented surfaces, as the CTA concentration was increased from 3 to 5 to 7 wt %, respectively. Interestingly, the viscosity of the precursor affected not only the final morphology of the spun product but also the surface pattern. The dents were broadened, and the number of dents were reduced when a higher viscosity precursor was used, likely because of the decreased solvent evaporation rate.

Porous structures were formed because of a combination of thermally induced phase separation and the breath figure mechanism. In this type of process, rapid solvent evaporation rapidly decreases the temperature at the surface of the jet. Once phase separation occurs, the evaporation of the solvent-rich phase (i.e., the polymer-poor phase) leaves behind voids that result in the formation of pores along the fiber.[12,20−24] Subsequently, ambient water vapor tends to condense on the cool surface of the polymer jet and forms into droplets as the surface temperature is further decreased, leaving porous imprints after the water evaporates.[25−27] Therefore, at a high polymer concentration, the number of dents was decreased because the temperature drop at the surface of the jet was not as extreme and only a small number of water droplets condensed. Delayed evaporation will also result in a higher solvent content in the jet, meaning that improved elongation can be obtained. Therefore, the dented surface was stretched during elongation to form long dimples with a shallow pattern. As a result, some of the electrospun fibers had a twisted appearance.

Employing a high humidity environment during electrospinning can also increase the extent of water vapor condensation.[5,19] To evaluate this effect, relative humidity values of 35, 50, and 70% were used to synthesize porous CTA fibers. Figure 1a,d,g demonstrates that the depth of the surface pattern was increased to form pores as the humidity was increased. Furthermore, the number of pores was increased, and these pores were uniformly distributed over the surfaces of the electrospun fibers. This phenomenon was also observed when using a high-viscosity polymer precursor. A higher pore concentration on the beads was obtained from a precursor containing 5 wt % CTA, whereas dented surfaces were present on the surfaces of fibers prepared from a precursor containing 7 wt % CTA, as can be seen in Figure 1.

2.2. Size-Controlled CTA Fibers by Secondary Polymer Addition. The final morphology of the electrospun fibers is significantly affected by the elongation of the polymeric precursor and by the amount of water vapor condensed on the jet surface. In particular, the ambient humidity determines the quantity of pores on the fiber surfaces, although pores will only form on exposed surfaces such as the exteriors of spherical particles and beads. In contrast, pores are typically not found on the fiber surfaces, likely because there is not enough space for phase separation and because the solvent rapidly evaporates from these thin surfaces, meaning that water vapor does not have time to occupy the fiber jet surface before the solvent evaporates and a solid fiber is formed. Therefore, secondary polymer addition, which can tune the Taylor cone shape and postpone the solvent evaporation, is extremely helpful in this process. A

DOI: 10.1021/acsomega.8b00695
ACS Omega 2018, 3, 8271−8277

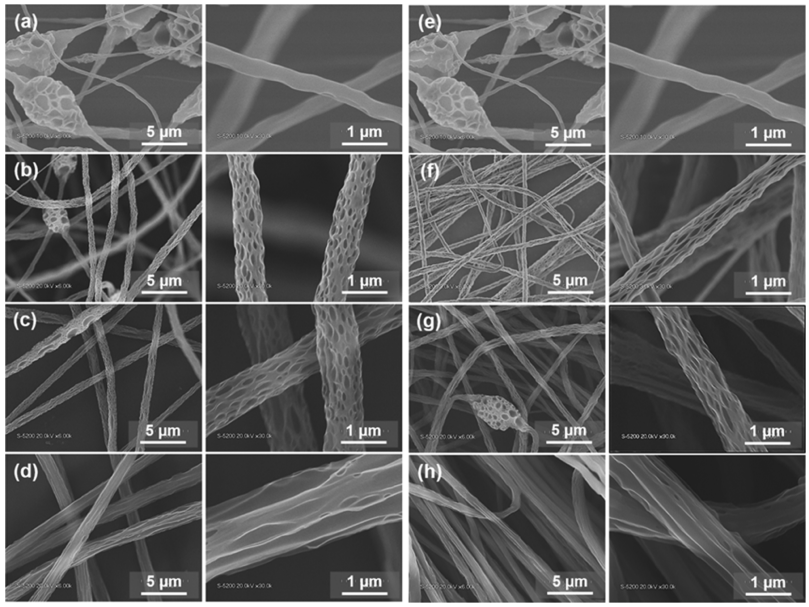

Figure 2. SEM images of porous fibers before immersion in 80 °C water for 3 h, prepared at a relative humidity of 70% from polymer precursors containing MC/EtOH ratios (vol/vol) of 90/10 as the solvent, 5 wt % CTA, and (a) 0 wt % PVP, (b) 2 wt % 10 kDa PVP, (c) 2 wt % 40 kDa PVP, and (d) 2 wt % 1300 kDa PVP. SEM images of porous fibers after immersion, made with the addition of (e) 0 wt % PVP, (f) 2 wt % 10 kDa PVP, (g) 2 wt % 40 kDa PVP, and (h) 2 wt % 1300 kDa PVP.

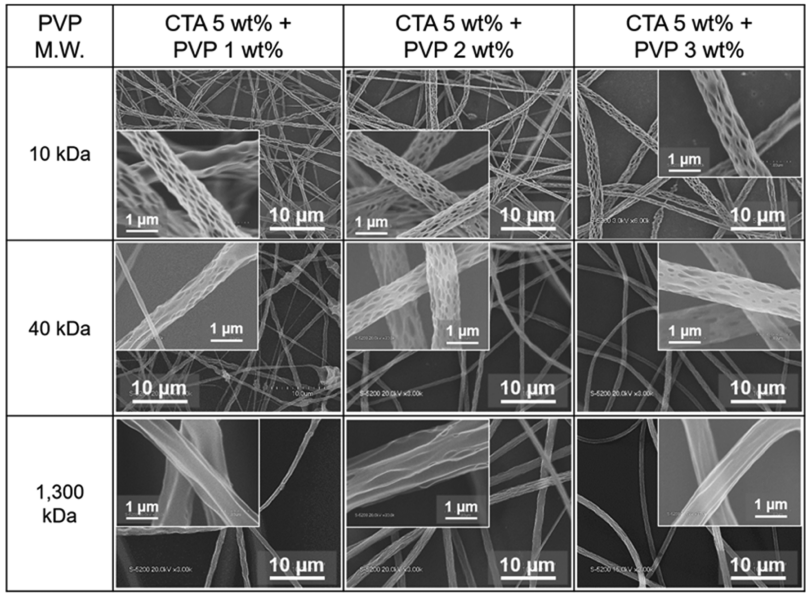

Figure 3. SEM images showing the effects of PVP concentration and molecular weight on porous morphology before immersion, applying a relative humidity of 70% in conjunction with 5 wt % CTA. High-resolution images are included as insets.

hydrophilic polymer such as polyvinylpyrrolidone (PVP) is optimal, especially if this polymer can be obtained in a variety of molecular weights to allow adjustment of the polymer precursor viscosity. This approach tends to prevent the formation of beads, and employing PVP also promotes the condensation of water vapor on the surface of the jet and slows solvent evaporation, as is evident from Supporting Information Figure S1.

On the basis of the polymer precursor viscosity after PVP addition, a solution containing 5 wt % CTA was selected for the fabrication of the composite fibers. This precursor was predicted to allow the formation of narrow composites with a definitive pore morphology. Figure 2 presents SEM images showing the effects of the PVP molecular weight on the porous morphology. It is evident that pores were uniformly formed on the surfaces of the beads and fibers upon adding the PVP. These pores tended to form cylindrical and slit shapes as a result of water evaporation during elongation of the polymeric fibers.[5] The application of a high voltage to the collector plate resulted in the precursor experiencing a strong attractive force, leading to significant elongation and therefore stretching the pores from spherical to oval shapes. The porous morphology was also affected by the molecular weight of the PVP, as shown in Figure 2a–d. The pores were lengthened as the PVP molecular weight was increased, with values of approximately 180 and 235 nm for the 10 and 40 kDa PVP, respectively. The

DOI: 10.1021/acsomega.8b00695
ACS Omega 2018, 3, 8271−8277

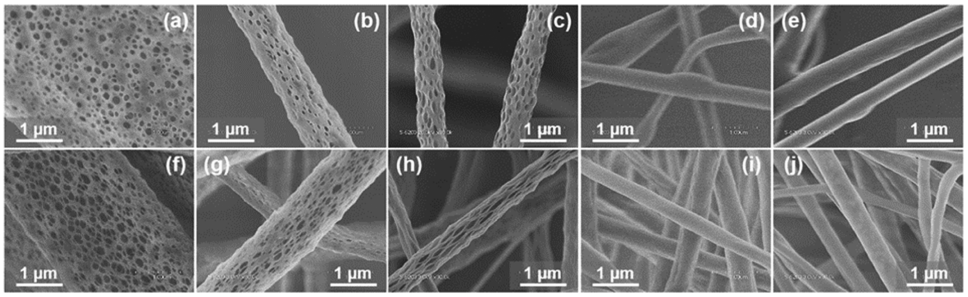

Figure 4. SEM images of spun polymers obtained from precursors containing 5 wt % CTA and 2 wt % 10 kDa PVP at a relative humidity of 70%, with MC/EtOH ratios (vol/vol) of (a,f) 100/0, (b,g) 95/5, (c,h) 90/10, (d,i) 85/15, and (e,j) 80/20, both (a−e) before immersion and (f−j) after immersion.

addition of the highest molecular weight PVP (1300 kDa) formed long, slit-shaped, shallow pores. The PVP tended to reach the surface of the jet and the higher molecular-weight-producing longer pores. Furthermore, the 1300 kDa PVP slowed the solvent evaporation rate and therefore promoted the formation of shallow pores.

Pure CTA fibers are required for filtration applications, and therefore the prepared fibers were purified by immersion process prior to filtration trials. The fiber and pore morphologies did not show any significant changes after the immersion process, as shown in Figure 2e−h. Using the low and medium molecular-weight PVP, the lengths of the pores were increased from 180 and 235 to 250 and 285 nm, whereas the fiber diameters were slightly decreased from 780 and 850 to 630 and 710 nm, respectively. These results confirm that the PVP migrated and accumulated on the surfaces of the spun fibers.

Figure 3 demonstrates that the porosity of the nanofibers was increased in proportion to the concentration of PVP, up to 2 wt %. However, at a higher concentration of PVP (i.e., 3 wt %), the porosity of the CTA nanofibers was significantly decreased because the solvent could not evaporate rapidly.

The PVP removal process evidently altered the porous structure, such that the pore diameters were decreased while the lengths were increased, as can be seen in Supporting Information Figure S2. This effect is attributed to stretching of the polymer when immersed in water during the PVP removal process. The PVP was firmly attached to the surfaces of the CTA fibers, including the pore surfaces, and so as it slowly dissolved in the water, it pulled at the fiber surfaces to create a stretching force that altered the porous morphology.

2.3. Size-Controlled CTA Fibers by Co-Solvent Addition. The other factor that may affect the morphology of the fibers is the solvent. To determine the boundary conditions at which porous or NP fibers would be obtained, various EtOH/MC volume ratios were evaluated using a precursor solution containing 5 wt % CTA and 2 wt % 10 kDa PVP. Figure 4a−e shows that the porosity was inversely proportional to the EtOH concentration in the precursor. A polymer precursor made using 100 vol % MC produced a highly porous ribbon fiber. During this trial, a skin was formed after the jet left the needle and the MC was evaporated, after which the tube formed by the skin collapsed under atmospheric pressure to produce a wide, flat, ribbonlike fiber.[13,28] In addition, pores were formed from the imprints of the evaporating solvent and water vapor.

The addition of EtOH reduced the evaporation rate of the solvent, and mixtures of spiny, porous ribbons and straight porous nanofibers were formed when using 5 vol % EtOH in the precursor. Increasing the EtOH concentration to 10 vol % produced solely the straight porous nanofibers. In this case, the formation of hollow shells that subsequently collapsed did not occur because there was no sudden solvent evaporation. The addition of a higher EtOH concentration further slowed the solvent evaporation, and therefore straight fibers were also obtained from solvents containing 15 and 20 vol % EtOH. Pores could not be observed in these fibers because the slow evaporation of the solvent prevented phase separation. In the case of porous fiber, Figure 4f−h confirms that the pores were increased in size following the immersion process. Whereas, in the case of straight fiber, pores still cannot be observed even after immersion process, as shown in Figure 4i,j. It confirms that the high concentration of EtOH produced dense fiber.

2.4. Aerosol Filtration Performance of Nonwoven CTA Fiber Mats. The effects of pore formation on the fiber surfaces on the filtration performance have not yet been studied in detail. To date, the performance of mats with and without pores has been examined without considering the size of the fibers. Generally, porous fibers will have a much smaller diameter compared to NP fibers when prepared using the same concentration of polymer because of the low viscosity of the polymer precursor and the rapid evaporation of the solvent. However, it is unclear whether collection efficiency is improved because of the smaller fiber diameter or the presence of pores. Therefore, in this study, fibers having similar sizes were prepared and assessed to confirm the effect of pores.

Aerosol particle permeation tests and pressure-drop measurements were performed using multilayer air filters composed of straight microfiber mats and nanostructured CTA fibers, employing an atmosphere containing dust particles with diameters in the range of 0.03−0.3 μm. Various particle-capture mechanisms, including diffusion, MPPS, interception, and inertial impaction could be investigated by varying the size of the dust.

Because the multilayer filters were quite inhomogeneous, the basis weights of the filters were used as a parameter in these trials. As noted, the basis weight was 3.35−3.54 g m^{-2}. It has been widely reported that the filtration performance is greatly affected by the filter morphology, particularly by the fiber diameter. In the present study, we found that the presence of pores on the surfaces of single fibers enhanced the aerosol filtration performance, as shown in Figure 5a,b. Interestingly, filter mats containing porous fibers exhibited outstanding particle-collection efficiency for all dust particle sizes, even within the MPPS region. Generally, particle collection efficiency at MPPS region is less than 85%, even for filter-

DOI: 10.1021/acsomega.8b00695
ACS Omega 2018, 3, 8271−8277

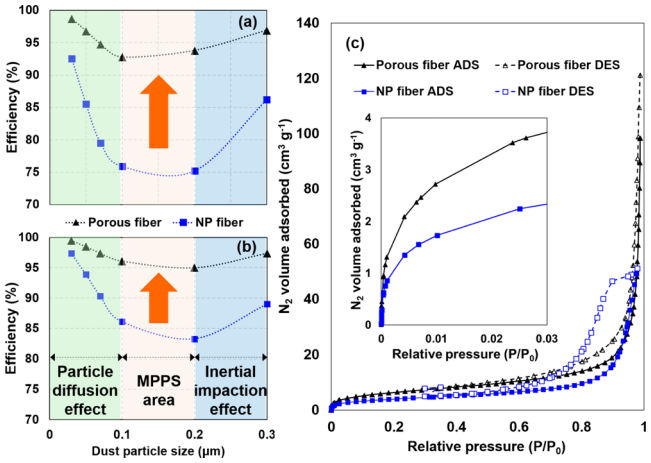

Figure 5. Effects of pores on the penetration of various aerosol particles at a face velocity of (a) 5.3 and (b) 1.4 cm s^{-1}. (c) N_2 ADS–DES isotherms of porous and NP fibers prepared from precursors containing 5 wt % CTA and 2 wt % 10 kDa PVP. Monolayer gas ADS data are included as an inset to (c).

containing nanofiber.[3] However, with the introduction of porous fiber, values of approximately 95 and 93% were obtained at face velocities of 1.4 and 5.3 cm s^{-1}, respectively. The particle capture efficiencies via the diffusion mechanism were also exceptional, with values as high as 99 and 99.5% for face velocities of 1.4 and 5.3 cm s^{-1}, respectively. The interception and inertial impaction mechanism also resulted in very high efficiencies of approximately 97% for both face velocities. These values were about 18% higher than the efficiencies obtained with NP fibers having the same diameter.

The parameters of porous and NP multilayer filters, including size distribution, filter thickness, and solid volume fraction were similar, as shown in Supporting Information Figure S3 and Table S1. Therefore, it can be concluded that the improved aerosol particle collection efficiency noted above can likely be attributed to the presence of pores on the entire surfaces of single nanofibers, which nearly doubled the surface area of the fibers.[29] The surface areas of the porous and NP fibers were determined using the Brunauer–Emmett–Teller method and found to be approximately 23.5 and 14.3 m^2 g^{-1}, respectively. The N_2 adsorption (ADS)–desorption (DES) curves in Figure 5c indicate that both the porous and NP fibers generated type-II isotherm curves, indicating that they were macroporous materials. In the case of the NP fibers, the macropores are ascribed to voids between nonwoven fibers. In contrast, the macropores on the porous fibers are composed of both pores on the surfaces of single fibers and voids among nonwoven fibers. The NP fibers produced a much wider hysteresis gap than that of the porous fibers, equivalent to type H2 hysteresis.[30] This hysteresis reflects the delayed condensation and pore blocking/percolation effects because of the presence of a disordered pore network within the nonwoven mat. In the case of the porous fibers, hysteresis was not observed, indicating that the pores were completely accessible as a result of the channels formed on the surfaces of single fibers.

A packing filter containing porous nanofibers generated a pressure drop on the order of 140 Pa, close to twice that obtained using the NP fibers (65 Pa). This result can likely be attributed to the large number of dust particles that were collected and eventually blocked the pores of the fibers.

3. CONCLUSIONS

The synthesis of porous CTA nanofibers via electrospinning was evaluated in detail, using thermally induced phase separation and the breath figure mechanism in conjunction with MC. Ambient humidity and the concentrations of the PVP secondary polymer and EtOH cosolvent were adjusted to control the fiber diameter and porosity. The PVP was subsequently removed by immersing the fibers in warm water to prevent morphological change of fiber during filtration application. Porous and NP fibers having similar sizes were compared to elucidate the effect of pores on aerosol filtration performance. Trials with a variety of dust particle sizes demonstrated that the porous fiber particle-capture efficiencies based on particle diffusion, inertial impaction, and interception were superior. The efficiency of the porous fibers within the MPPS region was also significantly improved (to 95%), providing evidence that the presence of dynamic pores can greatly improve particle capture.

4. METHODS

4.1. Electrospinning to Produce Nonwoven Fibers Mats. Precursor solutions were made by dissolving CTA (Sigma-Aldrich, St Louis, MO, USA) and PVP (M_w = 10, 40, or 1300 kDa; Sigma-Aldrich, St Louis, MO, USA), as a secondary polymer, in mixtures of MC and EtOH (containing 0–20 vol % EtOH). These solutions were used to prepare porous fibers via electrospinning. The PVP was heated at 80 °C for 1 h to reduce its moisture content prior to use. The electrospinning system was composed of a gas-tight syringe (1000 μm, Hamilton, Reno, NV, USA) with a 27G needle, a syringe pump (PHD 2000, Harvard Apparatus, Holliston, MA, USA), two high-voltage generators with positive and negative polarity (HER-30P1, Matsusada Precision Inc., Shiga, Japan), a temperature controller (PAU-300S-HC, Apiste Corp., Osaka, Japan), a heater (HLT-61, Hitachi Ltd., Tokyo, Japan), a humidity controller (AHCU-1, KITZ Corp., Chiba, Japan), a chamber, and an aluminum collector plate. Typically, a positive voltage of 10 kV was applied to the syringe needle to obtain a stable liquid jet, and a counter voltage of −4 kV was applied to the aluminum collector plate. The precursor solution was pumped at 4 μL min^{-1}. To evaluate the phase separation and the breath figure mechanism, trials were run with the chamber environment conditioned to relative humidities of 35, 50, or 70%. The syringe position was set at a fixed distance of 12 cm from the collector plate. The morphology of the porous fibers mats in the high humidity environment was stabilized by immersing the fibers in 80 °C water for 3 h.

4.2. Characterization of Precursors, Porous Fibers Mats, and Aerosol Filtration Performance. The viscosity of the aqueous solutions was evaluated using a Brookfield DV-III rheometer (Brookfield, Middleboro, MA, USA). The morphologies of the spun porous fiber mats were observed by field-emission SEM (S-5000, 20 kV, Hitachi High-Tech. Corp., Tokyo, Japan).

Aerosol filtration properties were assessed by electrospinning a precursor solution on the surface of a base filter to obtain multilayer filter membranes. Circular microfiber mats (Nippon Muki Co., Ltd., Tokyo, Japan) consisting a nonwoven fabric made of polypropylene with polyethylene terephthalate fibers, with a basis weight of 3.35–3.54 g m^{-2} and a diameter of 5.23 cm, were used as the base filters. The performance of each of the prepared multilayer filters was evaluated using atmospheric

DOI: 10.1021/acsomega.8b00695
ACS Omega 2018, 3, 8271–8277

dust particles with sizes in the range of 0.03−0.3 μm. These filters were exposed to isopropanol vapor overnight, prior to each measurement, to eliminate the effects of the electrostatic deposition of dust particles. Details of the measurement procedure have been provided in a previous publication.[2,3]

■ ASSOCIATED CONTENT

Supporting Information

The Supporting Information is available free of charge on the ACS Publications website at DOI: 10.1021/acsomega.8b00695.

Porous fiber formation during electrospinning, SEM images of porous fibers affected by PVP concentration and molecular weight, size distribution of porous and NP fibers, and parameters and aerosol filtration performances (PDF)

■ AUTHOR INFORMATION

Corresponding Author

*E-mail: ogit@hiroshima-u.ac.jp. Phone: +81-82-424-7850. Fax: +81-82-424-7850 (T.O.).

ORCID

Takashi Ogi: 0000-0003-3982-857X

Notes

The authors declare no competing financial interest.

■ ACKNOWLEDGMENTS

This research was supported by JSPS KAKENHI Grant-in-Aid numbers 26709061 and 16K13642 and by the Center for Functional Nano Oxides at Hiroshima University. We thank Michael D. Judge, MSc., from Edanz Group (www.edanzediting.com/ac) for editing a draft of this manuscript.

■ REFERENCES

(1) Wang, X.; Drew, C.; Lee, S.-H.; Senecal, K. J.; Kumar, J.; Samuelson, L. A. Electrospun Nanofibrous Membranes for Highly Sensitive Optical Sensors. *Nano Lett.* **2002**, *2*, 1273−1275.

(2) Balgis, R.; Kartikowati, C. W.; Ogi, T.; Gradon, L.; Bao, L.; Seki, K.; Okuyama, K. Synthesis and Evaluation of Straight and Bead-Free Nanofibers for Improved Aerosol Filtration. *Chem. Eng. Sci.* **2015**, *137*, 947−954.

(3) Bao, L.; Seki, K.; Niinuma, H.; Otani, Y.; Balgis, R.; Ogi, T.; Gradon, L.; Okuyama, K. Verification of Slip Flow in Nanofiber Filter Media through Pressure Drop Measurement at Low-Pressure Conditions. *Sep. Purif. Technol.* **2016**, *159*, 100−107.

(4) Wang, Z.; Zhao, C.; Pan, Z. Porous Bead-on-String Poly(Lactic Acid) Fibrous Membranes for Air Filtration. *J. Colloid Interface Sci.* **2015**, *441*, 121−129.

(5) Casper, C. L.; Stephens, J. S.; Tassi, N. G.; Chase, D. B.; Rabolt, J. F. Controlling Surface Morphology of Electrospun Polystyrene Fibers: Effect of Humidity and Molecular Weight in the Electrospinning Process. *Macromolecules* **2004**, *37*, 573−578.

(6) Bae, H.-S.; Haider, A.; Selim, K. M. K.; Kang, D.-Y.; Kim, E.-J.; Kang, I.-K. Fabrication of Highly Porous PMMA Electrospun Fibers and Their Application in The Removal of Phenol and Iodine. *J. Polym. Res.* **2013**, *20*, 158.

(7) Leong, M. F.; Chian, K. S.; Mhaisalkar, P. S.; Ong, W. F.; Ratner, B. D. Effect of Electrospun Poly(d,l-lactide) Fibrous Scaffold with Nanoporous Surface on Attachment of Porcine Esophageal Epithelial Cells and Protein Adsorption. *J. Biomed. Mater. Res., Part A* **2009**, *89*, 1040−1048.

(8) Li, Y.; Lim, C. T.; Kotaki, M. Study on Structural and Mechanical Properties of Porous PLA Nanofibers Electrospun by Channel-Based Electrospinning System. *Polymer* **2015**, *56*, 572−580.

(9) Li, L.; Jiang, Z.; Li, M.; Li, R.; Fang, T. Hierarchically Structured PMMA Fibers Fabricated by Electrospinning. *RSC Adv.* **2014**, *4*, 52973−52985.

(10) Bognitzki, M.; Czado, W.; Frese, T.; Schaper, A.; Hellwig, M.; Steinhart, M.; Greiner, A.; Wendorff, J. H. Nanostructured Fibers via Electrospinning. *Adv. Mater.* **2001**, *13*, 70−72.

(11) Zander, N. Hierarchically Structured Electrospun fibers. *Polymers* **2013**, *5*, 19−44.

(12) McCann, J. T.; Marquez, M.; Xia, Y. Highly Porous Fibers by Electrospinning into a Cryogenic Liquid. *J. Am. Chem. Soc.* **2006**, *128*, 1436−1437.

(13) Moon, S.; Choi, J.; Farris, R. J. Highly Porous Polyacrylonitrile/Polystyrene Nanofibers by Electrospinning. *Fibers Polym.* **2008**, *9*, 276−280.

(14) Yoon, Y. I.; Moon, H. S.; Lyoo, W. S.; Lee, T. S.; Park, W. H. Superhydrophobicity of Cellulose Triacetate Fibrous Mats Produced by Electrospinning and Plasma Treatment. *Carbohydr. Polym.* **2009**, *75*, 246−250.

(15) Han, S. O.; Son, W. K.; Youk, J. H.; Lee, T. S.; Park, W. H. Ultrafine Porous Fibers Electrospun from Cellulose Triacetate. *Mater. Lett.* **2005**, *59*, 2998−3001.

(16) Ramakrishna, S.; Fujihara, K.; Teo, W. E.; Lim, T. C.; Zuwei, M. *An Introduction Electrospinning and Nanofibers*; World Scientific Publishing Company: Singapore, 2005; p 101.

(17) Yun, K. M.; Suryamas, A. B.; Iskandar, F.; Bao, L.; Niinuma, H.; Okuyama, K. Morphology Optimization of Polymer Nanofiber for Applications in Aerosol Particle Filtration. *Sep. Purif. Technol.* **2010**, *75*, 340−345.

(18) Yun, K. M.; Hogan, C. J., Jr.; Matsubayashi, Y.; Kawabe, M.; Iskandar, F.; Okuyama, K. Nanoparticle Filtration by Electrospun Polymer Fibers. *Chem. Eng. Sci.* **2007**, *62*, 4751−4759.

(19) Huang, L.; Bui, N.-N.; Manickam, S. S.; McCutcheon, J. R. Controlling Electrospun Nanofiber Morphology and Mechanical Properties Using Humidity. *J. Polym. Sci., Part B: Polym. Phys.* **2011**, *49*, 1734−1744.

(20) Lin, J.; Ding, B.; Yu, J. Direct Fabrication of Highly Nanoporous Polystyrene Fibers via Electrospinning. *ACS Appl. Mater. Interfaces* **2010**, *2*, 521−528.

(21) Lu, J.-W.; Zhang, Z.-P.; Ren, X.-Z.; Chen, Y.-Z.; Yu, J.; Guo, Z.-X. High-Elongation Fiber Mats by Electrospinning of Polyoxymethylene. *Macromolecules* **2008**, *41*, 3762−3764.

(22) Kongkhlang, T.; Kotaki, M.; Kousaka, Y.; Umemura, T.; Nakaya, D.; Chirachanchai, S. Electrospun Polyoxymethylene: Spinning Conditions and Its Consequent Nanoporous Nanofiber. *Macromolecules* **2008**, *41*, 4746−4752.

(23) Gupta, A.; Saquing, C. D.; Afshari, M.; Tonelli, A. E.; Khan, S. A.; Kotek, R. Porous Nylon-6 Fibers via a Novel Salt-Induced Electrospinning Method. *Macromolecules* **2009**, *42*, 709−715.

(24) Pai, C.-L.; Boyce, M. C.; Rutledge, G. C. Morphology of Porous and Wrinkled Fibers of Polystyrene Electrospun from Dimethylformamide. *Macromolecules* **2009**, *42*, 2102−2114.

(25) Srinivasarao, M.; Collings, D.; Philips, A.; Patel, S. Three-Dimensionally Ordered Array of Air Bubbles in a Polymer Film. *Science* **2001**, *292*, 79−83.

(26) Megelski, S.; Stephens, J. S.; Chase, D. B.; Rabolt, J. F. Micro- and Nanostructured Surface Morphology on Electrospun Polymer Fibers. *Macromolecules* **2002**, *35*, 8456−8466.

(27) Lu, P.; Xia, Y. Maneuvering the Internal Porosity and Surface Morphology of Electrospun Polystyrene Yarns by Controlling the Solvent and Relative Humidity. *Langmuir* **2013**, *29*, 7070−7078.

(28) Koombhongse, S.; Liu, W.; Reneker, D. H. Flat Polymer Ribbons and Other Shapes Flat polymer ribbons and other shapes by electrospinning. *J. Polym. Sci. B Polym. Phys.* **2001**, *39*, 2598−2606.

(29) Li, X.; Teng, K.; Shi, J.; Wang, W.; Xu, Z.; Deng, H.; Lv, H.; Li, F. Electrospun preparation of polylactic acid nanoporous fiber membranes via thermal-nonsolvent induced phase separation. *J. Taiwan Inst. Chem. Eng.* **2016**, *60*, 636−642.

DOI: 10.1021/acsomega.8b00695
ACS Omega 2018, 3, 8271−8277

(30) Lowell, S.; Shields, J. E.; Thomas, M. A.; Thommes, M. *Characterization of Porous Solids and Powders: Surface Area, Pore Size and Density*; Springer: Netherlands, 2004; p 44.

DOI: 10.1021/acsomega.8b00695
ACS Omega 2018, 3, 8271−8277